Byproducts formed During Thiol-Acrylate Reactions Promoted by Nucleophilic Aprotic Amines: Persistent or Reactive?

Vasileios Drogkaris and Brian H. Northrop*[a]

The nucleophile-initiated mechanism of thiol-Michael reactions naturally leads to the formation of undesired nucleophile byproducts. Three aza-Michael compounds representing nucleophile byproducts of thiol-acrylate reactions initiated by 4-dimethylaminopyridine (DMAP), 1-methylimidazole (MIM), and 1,8-diazabicyclo[5.4.0]undec-7-ene (DBU) have been synthesized and their reactivity in the presence of thiolate has been investigated. Spectroscopic analysis shows that each nucleophile byproduct reacts with thiolate to produce a desired thiol-acrylate product along with liberated aprotic amines DMAP, MIM, or DBU, thus demonstrating that these byproducts are reactive rather than persistent. Density functional theoretical computations support experimental observations and predict that a β-elimination mechanism is favored for converting each nucleophile byproduct into a desired thiol-acrylate product, though an S_N2 process can be competitive (i.e. within <2.5 kcal/mol) in less polar solvents.

Introduction

Thiol-Michael reactions have been of significant interest over the past decade,[1] in large part because they exhibit the characteristics of "click" chemistry:[2] e.g. high yields, broad substrate scope and solvent tolerance, little to no byproduct formation, rapid kinetics, tolerance of oxygen, and straightforward purification. The desirable characteristics of thiol-Michael reactions have enabled these transformations to become an indispensable tool for a wide variety of applications such as the synthesis of polymers,[3] dendrimers,[4] cross-linked and shape memory networks,[5] hydrogels,[6] and vesicles[7] as well as for bioconjugation[8] and the functionalization of surfaces.[9] The mechanism of thiol-Michael reactions has been thoroughly investigated both experimentally[10] and computationally.[11] The two most prominent means of carrying out thiol-Michael reactions are by using either catalytic base or a nucleophile initiator.[1,10a,b] The base-catalyzed mechanism includes the deprotonation of the thiol by the base (Scheme 1, blue), which generates a thiolate that can in turn add to an activated double bond. The nucleophile-initiated mechanism proceeds via the nucleophilic addition of the initiator to a double bond creating a zwitterionic intermediate. This intermediate can deprotonate the thiol (Scheme 1, yellow) and thus initiate the thiol-Michael reaction. The selection of the initiator and the solvent dictates the mechanism that will generate the thiolate needed for entry into the catalytic anionic cycle of the addition mechanism (Scheme 1, green). For example, phosphines, when used as initiators, are known to proceed through the nucleophilic mechanism.[10a–b,d,11c–e] On the other hand, many amines can initiate the reaction through a base-catalyzed mechanism, a nucleophile-based mechanism or a combination of both mechanisms.[10a,c,11d] When amines are used, the nucleophilic pathway produces aza-Michael adducts which can negatively impact the reaction yields and complicate the purification of the products. There is evidence that suggests that even strongly basic amines, such as DBU,[10a] do not rely solely on the base-catalyzed mechanism. It is therefore important to investigate the degree to which the aza-Michael intermediates might impact the product formation.

Early reports[1b,10a–b,e,11d–e] cautioned against the use of high loading of nucleophile initiators in order to limit the formation

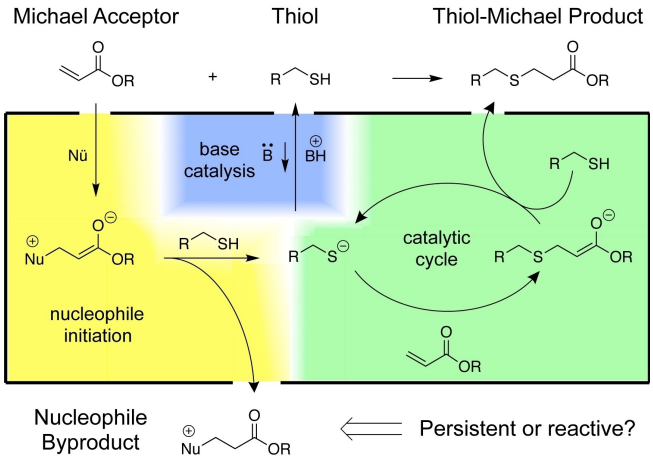

Scheme 1. Representation of the two most prominent means of forming catalytic thiolate along both nucleophile (yellow) and base (blue) pathways, each providing entry to the catalytic anionic cycle (green) that leads to thiol-Michael product formation. The nucleophile initiated pathway also results in the formation of nucleophile byproducts, some of which are persistent while others can be reactive depending on the nucleophile used.

[a] V. Drogkaris, Prof. B. H. Northrop
Department of Chemistry
Wesleyan University
52 Lawn Avenue, Middletown, CT 06459, USA
E-mail: bnorthrop@wesleyan.edu

Supporting information for this article is available on the WWW under https://doi.org/10.1002/cplu.202000590

of undesired nucleophile byproducts (Scheme 1). To evaluate the likelihood of forming undesired nucleophile byproducts we have previously investigated[12] the thiol-methyl acrylate reaction initiated by dimethylphenylphosphine (DMPP), hexylamine (HA), and diethylamine (DEA). These three initiators are known to promote the reaction predominantly via the nucleophilic pathway, therefore model systems of the thiol-methyl acrylate reaction were studied and the formation of initiator nucleophile byproduct was monitored. Minimal byproduct was detected by ^{1}H NMR spectroscopy, with byproduct formation accounting for a maximum of 4% of the crude mixture even when using up to a tenfold molar equivalent of the initiator. Nitrogen-centered compounds DEA and HA were observed to form undesired aza-Michael byproducts, however only in trace amounts (<4%) and only when present in large excess (e.g. 10 equiv) relative to thiol and methyl acrylate reactants. The choice of solvent also played a role in aza-Michael byproduct formation, with greater amounts of byproduct observed in less polar solvents. It is important to note, however, that no quantifiable amounts of aza-Michael byproducts could be observed when the amine-promoted thiol-methyl acrylate reactions were carried out using more commonly employed amounts of amine initiator, e.g. 1–10 mol%. Interestingly, no phosphonium ester byproducts could be detected by NMR spectroscopy when reactions were initiated by DMPP, regardless of initiator loading or solvent polarity. Experimental and computational studies[12] involving a model phosphonium ester byproduct revealed that the lack of any observable amount byproduct can be attributed to an elimination-addition pathway that takes place in the presence of thiolate, resulting in the formation of the desired thiol-Michael product. Aza-Michael byproducts resulting from nitrogen-centered nucleophiles DEA and HA are not able to follow a similar pathway and, therefore, can persist as undesired byproducts.

Herein we expand on previous work to include three aprotic amines – 4-dimethylaminopyridine (DMAP), 1-methylimidazole (MIM), 1,8-diazabicyclo[5.4.0]undec-7-ene (DBU) – that are commonly used in thiol-Michael reactions and whose initiation mechanism may include the nucleophilic pathway to some degree (see Schemes S1–S4 of the Supporting Information for the mechanism and calculated energetics of thiol-acrylate additions initiated by DMAP, MIM, and DBU acting as nucleophiles). Models of the aza-Michael adducts that can form during nucleophilie initiation of thiol-acrylate reactions involving these aprotic amines have been synthesized (**1**–**3**, Figure 1). It should be noted that attempts were made to include 1,4-diazabicyclo[2.2.2]octane (DABCO) as a fourth aprotic amine in this study. Despite extensive synthetic efforts, however, no nucleophile byproduct of DABCO or related bicyclic amine quinuclidine could be obtained.

Nucleophile byproducts **1**–**3** are charged quaternary species, similar to the phosphonium ester DMPP byproduct. As such it may be possible for quaternary aza-Michael byproducts to be converted into desired thiol-Michael products in the presence of thiolate along pathways similar to those investigated previously for phosphonium esters. Indeed experimental investigations do show that each of these model nucleophile

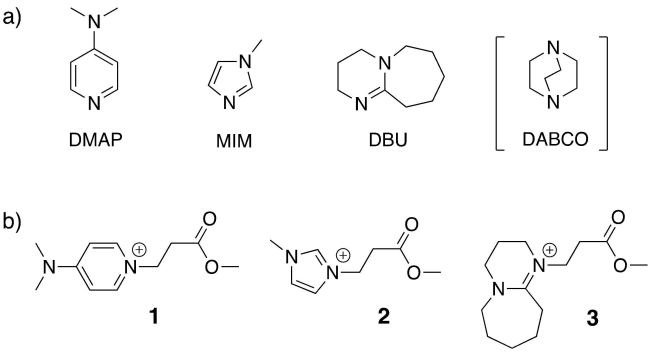

Figure 1. Chemical structures of (a) the nitrogen-centered nucleophiles DMAP, MIM, and DBU investigated in this study and (b) undesired nucleophile byproducts **1**–**3** that can form when thiol-methyl acrylate reactions are initiated by DMAP, MIM, and DBU, respectively. DABCO has also been investigated, however no nucleophile byproduct containing DABCO could be synthesized.

byproducts can be converted into desired thiol-methyl acrylate adducts in the presence of thiolate. Computational modeling in both polar (DMSO) and nonpolar ($CHCl_3$) solvents is used to explore the reaction pathways available for model compounds **1**–**3** to react with methane thiolate in an effort to determine which pathway is the most favorable for each nucleophile in each solvent type. Combined experimental and computational results provide a thorough picture of how these charged aza-Michael nucleophile byproducts are converted to desired thiol-Michael adducts in the presence of thiolate. The results provide a more complete understanding of the different roles that different nitrogen-centered bases/nucleophiles can play when promoting thiol-Michael reactions.

Results and Discussion

Synthesis and spectroscopy

The synthesis of model aza-Michael adducts **1**–**3** was carried out along one of two similar pathways (Scheme 2). Model byproduct **1** was prepared upon a reaction of DMAP with 3-

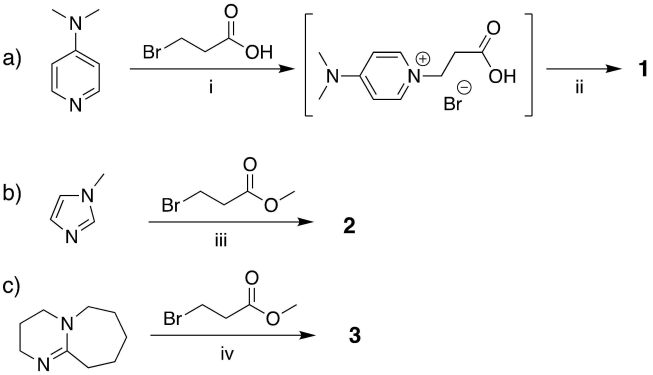

Scheme 2. Conditions: i) CH_3CN, 80 °C, ii) CH_3OH, HBr, reflux, iii) THF, 0 °C, iv) acetone.

bromopropionic acid followed by esterification under acidic conditions, as shown in Scheme 2a. Byproducts **2** and **3** could be prepared directly upon reaction of MIM or DBU with methyl 3-bromopropionate (Scheme 2b). The resulting ammonium salts **1**–**3** have exactly the same chemical structure as the nucleophile byproducts that may be formed when the same nitrogen-centered species are used to promote thiol-Michael reactions involving methyl acrylate. The only difference between model compounds **1**–**3** and those obtained during thiol-methyl acrylate reactions is the counterion: model compounds **1**–**3** are obtained as bromide salts whereas nucleophile byproducts formed during thiol-methyl acrylate reactions exist as thiolate salts as indicated in Scheme 1.

The model reaction summarized in Scheme 3 was designed to test whether model byproducts **1**–**3** can be converted into the desired thiol-Michael products. As noted above, for every equivalent of adduct formed during the nucleophile-initiated thiol-Michael reaction, one equivalent of thiolate is generated. Stoichiometrically equal amounts of nucleophile byproduct and thiolate are therefore expected to be present under normal thiol-Michael conditions. In order to model these conditions accurately, each of the aza-Michael adducts was reacted with an equimolar amount of the sodium salt of methyl 3-mercaptopropionate (**M3MP-**), under a nitrogen atmosphere in anhydrous $CDCl_3$. The thiolate was chosen with the aim that desired product **4** is symmetric, resulting in a less convoluted NMR spectrum of the crude reaction mixture. $CDCl_3$ was chosen as the solvent for this test reaction based on prior research[12] showing a greater likelihood of nucleophile byproduct formation in less polar solvents.

The DMAP byproduct **1** and its ^{1}H NMR spectrum are shown in Figure 2a. In the figure the proton signals for the DMAP and the methyl propionate moiety are highlighted in red and blue, respectively. Upon reacting byproduct **1** with the thiolate **M3MP-**, large upfield shifts corresponding to the methylene triplets can be observed, from 4.71 and 3.12 ppm in the byproduct to 2.80 and 2.61 ppm in the crude spectrum of the resulting product. A smaller but observable downfield shift is also observed for the methyl ester singlet, from 3.65 ppm in byproduct **1** to 3.68 ppm in the product. Residual DMAP can also be seen in the crude mixture, however no detectable amounts of DMAP byproduct **1** is observed spectroscopically. The two triplets and the singlet at 3.68 ppm in the crude spectrum match the signals of thiol-Michael product **4**.[12] This result indicates that residual thiolate present in DMAP-initiated

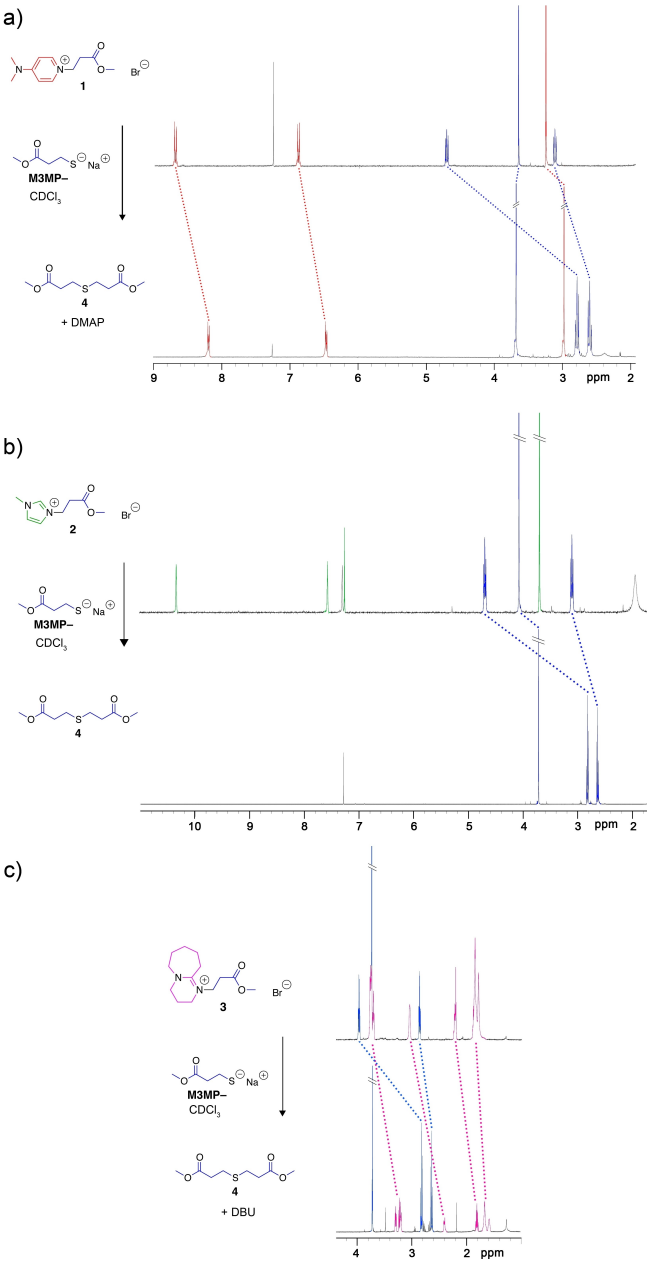

Figure 2. Partial ^{1}H NMR spectra showing the conversion of nucleophile byproducts **1**, **2**, and **3** into desired thiol-acrylate product **4** in the presence of **M3MP-**. Signals corresponding to DMAP in **1** are highlighted in red in (a), proton signals corresponding to MIM are highlighted in green in (b), and those corresponding to DBU are highlighted in purple in (c). Dashed lines indicate shifts of signals upon reaction with **M3MP-**.

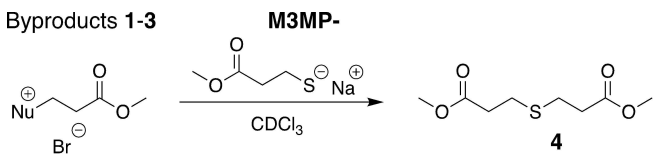

Scheme 3. Model reaction for investigating the potential consumption of nucleophile byproducts by thiolate to give symmetric thiol-acrylate product **4**. Thiolate **M3MP-** was prepared by treating methyl 3-mercapropropionate with sodium hydride and then transferring the freshly prepared salt to byproducts **1**–**3**.

thiol-acrylate reactions can indeed convert any undesired nucleophile byproduct into desired thiol-acrylate products.

Similar spectroscopic results were obtained for reactions involving MIM byproduct **2** and DBU byproduct **3** with thiolate **M3MP-**. The spectrum of the MIM adduct is shown at the top of Figure 2b, with the signals corresponding to the MIM moiety of byproduct **2** highlighted green and the proton signals corresponding to the methyl propionate moiety highlighted in blue. The methylene signals of **2** appear as triplets at 4.69 and 3.10 ppm which, after reacting with **M3MP-**, shift upfield to 2.82

and 2.63 ppm. The corresponding methyl ester singlet shifts from 4.07 ppm in the byproduct to 3.70 ppm in the spectrum of the crude mixture. As with DMAP, the undesired byproduct is converted cleanly into thiol-acrylate product **4** while no trace of residual **2** is observed. Spectroscopic support for the conversion of DBU byproduct **3** into thiol-acrylate product **4** in the presence of **M3MP-** is shown in Figure 2c. Diagnostic methylene triplets of byproduct **3** are observed to shift from 3.99 and 2.85 ppm to 2.82 and 2.63 ppm upon reaction with the thiolate. The methyl ester singlet in DBU byproduct **3** is not cleanly resolved as it overlaps with other methylene signals of the DBU moiety. Nonetheless, upon reaction with **M3MP-** the consumption of byproduct **3** results in the observation of a well-resolved methyl ester singlet of desired product **4** at 3.69 ppm.

Collectively, these experimental results constitute strong evidence that charged aza-Michael byproducts **1**–**3** formed during the initiation of thiol-acrylate reactions with DMAP, MIM, and DBU can react with the available thiolate that exists in the reaction mixture and yield desired thiol-acrylate products. In order to gain further insights into the mechanistic details of these reactions, the same model reactions were investigated computationally.

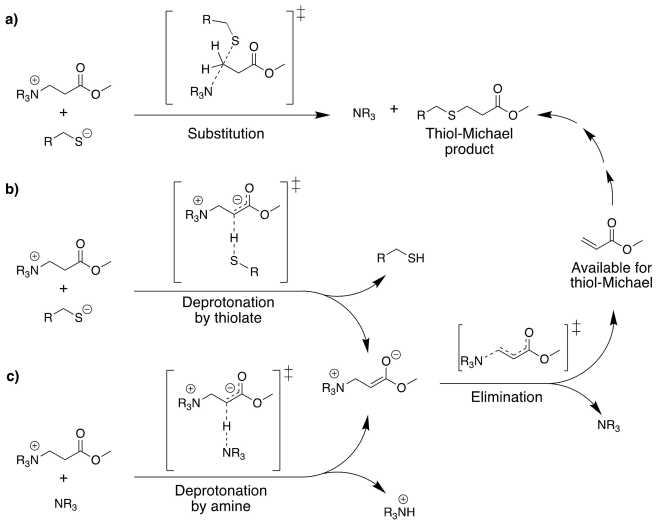

Scheme 4. Possible mechanisms for the conversion of nucleophile byproducts into desired thiol-Michael products include (a) direct S_N2 displacement by nucleophilic thiolate, (b) deprotonation by thiolate followed by elimination of nitrogen-centered species and subsequent thiol-Michael reaction, and (c) deprotonation by amine followed by elimination of the nitrogen-centered species and subsequent thiol-Michael reaction.

Computational modeling

^{1}H NMR results clearly demonstrate that model ammonium nucleophile byproducts **1**–**3** react with the conjugate base of methyl-3-mercaptopropionate to give thiol-Michael product **4**. Spectroscopic results do not, however, reveal the mechanism of this transformation. Previous research[12] involving phosphorous-centered nucleophile DMPP explored two mechanistic pathways that can convert undesired phosphonate ester byproducts into desired thiol-Michael products in the presence of thiolate: (i) an S_N2 displacement of DMPP from the phosphonium ester byproduct, and (ii) an elimination followed by addition pathway involving deprotonation of the phosphonium ester by thiolate followed by elimination of DMPP that also produces methyl acrylate, which can then undergo a productive thiol-methyl acrylate reaction. Computational modeling in solvent models for $CHCl_3$ and DMSO both showed that the elimination followed by addition pathway is favored over the S_N2 pathway by 15.9–17.7 kcal/mol, depending on the solvent.

A significant difference between prior investigations of DMPP and the current work involving nitrogen-centered species DMAP, MIM, and DBU is that each of the nitrogen-centered species is able to act as both a nucleophile and as a base. The basic nature of these species opens up an additional potential mechanistic pathway that's not available to DMPP, which is non-basic. In particular, it is possible that ammonium nucleophile byproducts **1**–**3** could be deprotonated by either thiolate or by residual base (DMAP, MIM, and DBU) present in the reaction mixture. The three reaction pathways that are capable of converting byproducts **1**–**3** into thiol-Michael product **4** and have been investigated computationally are summarized in Scheme 4. These three pathways are: (a) S_N2 displacement of the initial nitrogen-centered nucleophile, (b) deprotonation of the nucleophile byproduct by available thiolate followed by elimination and thiol-Michael addition, and (c) deprotonation of the byproduct by available base with subsequent elimination and thiol-Michael addition. Given that the pKa values of the four bases investigated range from approximately 7–12 it is possible that the most favored mechanistic pathway might not be the same for each of the byproducts **1**–**3**, and it's possible that the most favored pathway in each case could be solvent-dependent.

Computational investigations were also performed using DABCO as the aprotic amine. Interestingly, a transition state corresponding to nucleophilic attack of the acrylate π-bond by DABCO could not be located despite extensive exploration of the potential energy surface. This observation is noteworthy given the fact that all experimental attempts to synthesize a model nucleophile byproduct based on DABCO or related analogue quinuclidine were unsuccessful. Given these experimental and computational results it is reasonable to conclude that DABCO does not follow a nucleophilic pathway in thiol-acrylate reactions and is only capable of promoting such additions by acting as a base.

The most straightforward mechanism to investigate, given that it is a single step, is the direct S_N2 displacement of the nucleophile by thiolate attack at the β-carbon of the nucleophile byproduct, as shown in Scheme 4a. Table 1 summarizes the computational results for the nucleophilic attack of byproducts **1**–**3** resulting in the formation of thiol-Michael product **5** and nitrogen species DMAP, MIM, or DBU, respectively. Results are provided in solvent models for $CHCl_3$ and DMSO.

It is clear from the results in Table 1 that thiolate attack at the β-carbon nucleophile byproducts **1**–**3** is thermodynamically favored in both $CHCl_3$ ($-\Delta G^\circ = 28.1$–38.2 kcal/mol) and DMSO

Table 1. Relative free energies[a] calculated for the S_N2 transition state and the resulting thiol-Michael and NR_3 products.[b]

Nucleophile Byproduct	$CHCl_3$ S_N2 T.S.	Products	DMSO S_N2 T.S.	Products
1	18.0	−32.3	34.5	−13.1
2	16.4	−36.1	33.8	−15.8
3	20.7	−28.1	37.7	−8.5

[a] Relative energies ($\Delta G^{\ddagger}$, ΔG°) are given in kcal mol^{-1}. [b] See Scheme 4a.

(−ΔG° = 8.5–16.0 kcal/mol). Computational results therefore indicate there is a strong thermodynamic driving force for the conversion of a thiolate/nucleophile byproduct salt into desired thiol-Michael product and starting nucleophile by the S_N2 mechanism. Computations also indicate that the S_N2 reaction is significantly more exergonic in $CHCl_3$ than in DMSO on account of the fact that starting materials, i.e. thiolate and nucleophile byproducts **1**–**3**, are charged species while the products of the reaction, i.e. **5** and nitrogen species, are neutral. Relative to neutral products, the charged reactants are destabilized to a greater extent in less polar solvents such as $CHCl_3$ than in more polar solvents such as DMSO.

Transition state Gibbs free energies ($\Delta G^{\ddagger}$) for the S_N2 reaction are also found to be significantly lower in $CHCl_3$ than in DMSO. This result may also be expected on account of each solvent's ability to stabilize the separate charges of the reactants versus the net-neutral S_N2 transition state. The lower transition state free energies in $CHCl_3$ are also in line with the Hammond postulate given the greater exergonicity of the reaction in the less polar solvent and indicate an earlier, more reactant-like transition state. Comparisons of reaction energetics in different solvents are important given that it is possible different solvents may favor different pathways for converting nucleophile byproducts into desired thiol-Michael products.

Table 2 provides a summary of the reaction energetics for deprotonation of the nucleophile byproduct by available thiolate followed by elimination and thiol-Michael addition (Scheme 4b). Overall reaction energetics are again predicted to be more favorable in $CHCl_3$ than DMSO for the thiolate deprotonation followed by nucleophile elimination pathway. In fact, elimination of DBU following thiolate deprotonation of nucleophile byproduct **3** is predicted to be endergonic by ΔG° = 0.4 kcal/mol in DMSO. By contrast, results in $CHCl_3$ are all exergonic by 19.0–29.0 kcal/mol. The difference in overall reaction free energies can again be attributed to each solvent's ability to stabilize charged species versus neutral products. It is interesting to note that the difference in overall reaction free energies in $CHCl_3$ versus DMSO (ΔG°_{DMSO}–ΔG°_{CHCl3}) is approximately 20 kcal/mol for both the S_N2 pathway (Scheme 4a) and the thiolate deprotonation followed by elimination pathway (Scheme 4b).

While computations predict that overall reaction energetics are quite different in the two solvents investigated, the rate-determining step along the Scheme 4b pathway is predicted to be the same for both solvents. Specifically, results in both $CHCl_3$ and DMSO predict that the rate-determining step along the Scheme 4b pathway is the initial deprotonation of nucleophile byproducts **1**–**3** by thiolate. The one possible exception is deprotonation of DBU byproduct **3** in DMSO, where the deprotonation and elimination transition states are within computational error of each other ($\Delta G^{\ddagger}$ = 22.5 vs 22.1 kcal/mol, respectively). It is also worth noting that rate-determining steps along the Scheme 4b pathway are lower in $CHCl_3$ than DMSO by approximately 6.0–8.6 kcal/mol. Computational results suggest that, in $CHCl_3$, deprotonation of nucleophile byproducts **1**–**3** is rather facile ($\Delta G^{\ddagger} \leq$ 16.4 kcal/mol) and leads to rapid elimination to give products thiol, methyl acrylate, and eliminated nucleophile.

Finally, Table 3 summarizes computational results for the pathway summarized in Scheme 4c, which involves deprotonation of nucleophile byproducts **1**–**3** by their respective nitrogen species, followed by elimination similar to Scheme 4b (as indicated by the pathways converging). Three key conclusions can be drawn from the data summarized in Table 3. First and foremost, computational investigations predict that none of the deprotonation followed by elimination pathways shown in Scheme 4c are thermodynamically favored in either solvent model. Overall reaction free energies are endergonic by ΔG° = 3.4–11.0 kcal/mol in $CHCl_3$ and by ΔG° = 2.2–9.4 kcal/mol in DMSO. Second, in each solvent, transition state free energies for the deprotonation of nucleophile byproducts **1**–**3** by their respective nitrogen-centered base trend with the pK_a of that

Table 2. Relative free energies[a] calculated for the reaction pathway summarized in Scheme 4b.

Nucleophile Byproduct	Thiolate Deprotonation T.S.	Zwitterion Intermediate	Elimination T.S.	Products
1 ($CHCl_3$)	16.4	−0.5	1.4	−23.2
2 ($CHCl_3$)	14.0	−1.6	2.1	−27.0
3 ($CHCl_3$)	13.9	1.5	2.6	−19.0
1 (DMSO)	22.4	15.9	18.8	−4.3
2 (DMSO)	22.5	16.0	19.4	−7.0
3 (DMSO)	22.5	17.3	22.1	0.4

[a] Energies ($\Delta G^{\ddagger}$, ΔG°) are given in kcal mol^{-1} and are relative to reactants for each pathway. A graphical plot of the reaction energetics in both solvents is provided in the Supporting Information.

Table 3. Relative free energies[a] calculated for the reaction pathway that begins with deprotonation of byproducts **1**–**4** by nitrogen-centered bases, as summarized in Scheme 4c.

Nucleophile Byproduct	Base Deprotonation T.S.	Zwitterion Intermediate	Elimination T.S.	Products
1 ($CHCl_3$)	24.9	23.1	33.3	9.2
2 ($CHCl_3$)	27.7	27.3	38.6	11.0
3 ($CHCl_3$)	17.9	17.7	26.5	3.4
1 (DMSO)	25.7	25.6	30.3	7.2
2 (DMSO)	29.0	28.8	35.8	9.4
3 (DMSO)	19.3	19.1	23.9	2.2

[a] Energies ($\Delta G^{\ddagger}$, ΔG°) are given in kcal mol^{-1} and are relative to reactants for each pathway. A graphical plot of the reaction energetics in both solvents is provided in the Supporting Information.

residual base. For example, deprotonation of byproduct **3** by DBU is predicted to have the lowest transition state Gibbs free energy ($\Delta G^{\ddagger} = 17.9$ and 19.3 kcal/mol in $CHCl_3$ and DMSO, respectively) while deprotonation of byproduct **2** by MIM is predicted to have the highest transition state Gibbs free energy ($\Delta G^{\ddagger} = 27.7$ and 29.0 kcal/mol in $CHCl_3$ and DMSO, respectively). This observation highlights the greater variability in the behavior of nitrogen-centered compounds when used to promote thiol-Michael reactions relative to phosphorus-centered nucleophiles, which are non-basic and do not follow a pathway analogous to that shown in Scheme 4c.[10a–b,11c–e,12]

Third, in both $CHCl_3$ and DMSO, the rate-determining step along the Scheme 4c pathway is predicted to be nucleophile elimination. This is in contrast to the Scheme 4b pathway, where deprotonation of nucleophile byproducts by thiolate was the rate-determining step. Similarly, relative to reactants in each case, the formation of a protonated ammonium and zwitterion intermediate along pathway Scheme 4c is predicted to be less energetically favorable than the formation of the same zwitterion and thiol along pathway Scheme 4b. This difference in rate-determining step and the energetic difference of zwitterion formation along the two pathways is not attributed to the relative pK_a values of the nitrogen-centered species versus that of methyl mercaptan. After all, the pK_a of methyl mercaptan (~10.4) lies approximately in the middle of the range spanned by DMAP, MIM, and DBU (7–12). Instead the difference is likely a reflection of the greater separation of charge that occurs along the pathway shown in Scheme 4c versus that in Scheme 4b. Deprotonation of the nucleophile byproduct by its neutral nitrogen-centered base incurs the energetic penalty of forming a zwitterion and formally positive ammonium species. By contrast, deprotonation of the byproduct by thiolate along pathway Scheme 4b involves a consolidation of charge as the ammonium byproduct reacts with a negatively charged thiolate to produce the same zwitterion and a neutral thiol.

Overall, computational results suggest that the deprotonation followed by elimination pathway involving thiolate as a base (Scheme 4b) is, in general, energetically preferred over the pathway involving nitrogen species as bases (Scheme 4c). The one possible exception to this observation centers on conversion of DBU byproduct **3** into thiol-acrylate product **5** in DMSO, where the rate-determining steps along the Scheme 4b pathway (22.5 kcal/mol) is only 1.4 kcal/mol more favorable than along the Scheme 4c pathway (23.9 kcal/mol). Computational results therefore predict that, in DMSO, deprotonation of DBU byproduct **3** by residual DBU may be competitive with deprotonation of **3** by thiolate. In all other cases investigated deprotonation by residual thiolate is predicted to be more favored by ≥ 7.9 kcal/mol.

While computational results predict that pathway Scheme 4b is generally more favorable than pathway Scheme 4c in both solvents modeled, comparisons of the thiolate deprotonation followed by nucleophile elimination pathway and the direct S_N2 pathway are found to have greater solvent dependency. Computational modeling shows a clear preference for the thiolate deprotonation pathway (Scheme 4b) when the solvent model is DMSO. Comparing the DMSO results in Tables 1 and 2 reveals that the rate-determining step of the thiolate deprotonation pathway is predicted to be more favorable than the S_N2 pathway by 11.3–15.2 kcal/mol. In a less polar solvent such as $CHCl_3$, however, the Gibbs free energy differences between the thiolate deprotonation and the S_N2 pathways are notably smaller. In the case of DMAP nucleophile byproduct **1**, for example, the rate-determining step along the thiolate deprotonation pathway has a Gibbs free energy barrier of 16.4 kcal/mol while the Gibbs free energy barrier for S_N2 displacement is 18.0 kcal/mol. This predicted difference of only 1.4 kcal/mol suggests that in $CHCl_3$ the thiolate deprotonation and S_N2 displacement pathways are likely competitive, with the thiolate deprotonation pathway being followed approximately 91% of the time and the S_N2 pathway accounting for the other 9% at 298 K.[13] For the MIM nucleophile byproduct **2** the difference between the two pathways is 2.4 kcal/mol, again in favor of the thiolate deprotonation pathway. This difference in calculated Gibbs free energy barriers is slightly larger than in the case of DMAP, however it may still be possible for the S_N2 pathway to compete with thiolate deprotonation (approximately 1.7% versus 98.3% at 298 K) during the conversion of byproduct **2** into desired thiol-Michael product.[13] Considering DBU nucleophile byproduct **3**, however, the difference between the thiolate deprotonation and S_N2 pathways grows to a calculated 6.8 kcal/mol. Computations therefore indicate that the conversion of nucleophile byproduct **3** into desired thiol-Michael product is predicted to follow the thiolate deprotonation pathway in less polar solvents such as $CHCl_3$ and the S_N2 pathway will not be competitive. Figure 3 provides a summary of these insights provided from computational investigations along with the calculated structures of rate-determining step transition state geometries for each byproduct in both solvent models.

Conclusion

Model systems representing nucleophile byproducts that can be formed during thiol-acrylate reactions initiated by DMAP, MIM, or DBU have been synthesized and their reactivity with methyl 3-mercaptoproprionate has been investigated experimentally as well as computationally. Spectroscopic studies reveal that each unwanted nucleophile byproduct reacts completely with the methyl 3-mercaptoproprionate to give a desired thiol-acrylate product and a liberated aprotic amine base (DMAP, MIM, or DBU). These model reactions indicate that concerns regarding the accumulation of unwanted nucleophile byproducts during thiol-Michael reactions promoted by aprotic amines are unwarranted. The results also highlight key differences between using aprotic amines to promote thiol-Michael reactions versus using protic amines, e.g. diethylamine, hexylamine. Specifically, protic amines are able to undergo aza-Michael reactions and result in unwanted nucleophile byproducts that are persistent, whereas aza-Michael byproducts formed from aprotic amines are reactive species that are converted into desired thiol-Michael products in the presence of residual thiolate. Computational modeling supports exper-

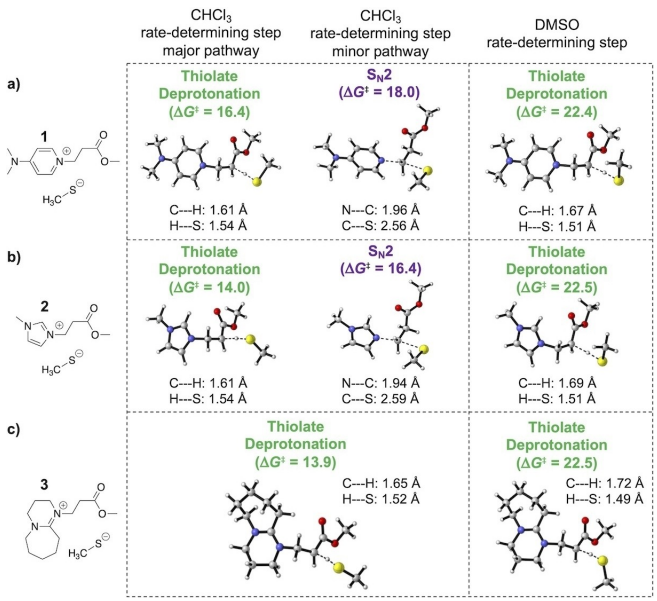

Figure 3. Structures of rate-determining step transition state geometries for the reaction of methane thiolate with DMAP nucleophile byproduct **1** (a), MIM nucleophile byproduct **2** (b), and DBU nucleophile byproduct **3** (c) as obtained from computational modeling. Dashed lines indicate bonds being broken/formed, with bond distances provided in angstroms. Transition state Gibbs free energies relative to starting reactants are provided in kcal/mol. While thiolate deprotonation is the major pathway for the three nucleophile byproducts in both solvents investigated, the S_N2 pathway provides an alternative, minor pathway for byproducts **1** and **2** in less polar solvents such as $CHCl_3$.

imental observations in that the conversion of nucleophile byproducts into thiol-acrylate products and recovered aprotic amines is predicted to be exergonic in all cases. Mechanistic analysis reveals that the most favored mechanism for the conversion involves deprotonation of the nucleophile byproduct by thiolate followed by elimination of the aprotic amine and a subsequent thiol-acrylate reaction. There are, however, subtle differences between the different aprotic amines and their reactivity in polar (DMSO) versus less polar ($CHCl_3$) solvents that enable alternative pathways to be competitive in some cases. In particular, while thiolate deprotonation is predicted to be preferred, an alternative S_N2 pathway may be competitive in less polar solvents. Overall the cumulative results provide further evidence that researchers who would like to take advantage of the many valuable attributes of thiol-Michael reactions can initiate these useful transformations with aprotic amines without needing to worry about the accumulation of undesired aza-Michael nucleophile byproducts.

Experimental Section

Materials and Reagents

4-Dimethylaminopyridine was purchased from Oakwood Chemical. 1-Methylimidazole was purchased from Sigma Aldrich. 1,8-Diazabicyclo[5.4.0]undec-7-ene and methyl-3-mercapto-propionate were purchased from Acros Organics. Methyl 3-bromopropionate was purchased from Combi-Blocks. 3-Bromopropionic acid was purchased from Chem-Impex International. All chemicals were used as received. Deuterated solvents were purchased from Cambridge Isotope Laboratories. Reagent-grade solvents were dried using an Innovative Technologies SPS-400-5 solvent purification system. Reactions were carried out under an inert atmosphere of N_2(g) unless otherwise noted. Thin layer chromatography (TLC) was carried out on aluminum-backed sheets coated with silica gel 60 with fluorescent indicator F254. Visualization of TLC plates was performed using a UV/vis lamp and/or by staining with I_2(s) or *p*-anisaldehyde solution. All ^{1}H and ^{13}C NMR spectra were recorded on a Varian Mercury (300 and 75 MHz, respectively) or Varian Unity (500 and 125 MHz, respectively) spectrometer using residual solvent as the internal standard. All chemical shifts are reported using the δ scale. All coupling constants are reported in Hertz (Hz). High-resolution ESI mass spectrometric analysis was performed at the University of Illinois, Urbana-Champaign Mass Spec Facility.

Synthesis and Characterization

1: To a solution of 4-dimethylaminopyridine (0.88 g, 7.2 mmol) in acetonitrile (20 mL), 3-bromopropionic acid (0.74 mL, 7.2 mmol) was added under an inert atmosphere and the reaction was stirred at 80 °C overnight. The solution was then allowed to cool down to room temperature. A precipitate was formed and was washed with acetonitrile and diethyl ether. The precipitate was then dissolved in methanol (15 mL), a small amount of concentrated HBr was added, and the solution was refluxed overnight. The solvent was then removed under reduced pressure and the desired dimethylaminopyridinium byproduct was precipitated from a mixture of DCM and EtOAc as a white solid (1.3 g, 62%). Melting point: 166–168 °C. TOF MS ES (*m/z*) $[M]^+$ calculated for $C_{11}H_{17}N_2O_2$, 209.1290, found 209.1293. ^{1}H NMR ($CDCl_3$, 300 MHz): δ ppm 8.70 (d, 2H), 6.89 (d, 2H), 4.71 (t, 2H), 3.65 (s, 3H), 3.25 (s, 6H), 3.12 (t, 2H); ^{13}C NMR ($CDCl_3$, 125 MHz): δ ppm 171.49, 156.38, 143.40, 107.81, 53.38, 52.23, 40.43, 35.05.

2: A solution of 1-methylimidazole (148 mg, 1.8 mmol) in THF (10 mL) was cooled down to 0 °C under an inert atmosphere and methyl 3-bromopropionate (0.196 mL, 1.8 mmol) was added. The reaction mixture was allowed to warm up to room temperature slowly and stir for 3 hours. The resulting precipitate formed was removed by filtration and washed with diethyl ether. The solvent of the filtrate was removed under reduced pressure and the product was purified by column chromatography on silica gel using a gradient starting with acetone and increasing to 9:1 acetone: methanol. The desired methylimidazolium byproduct was isolated as a colorless liquid (200 mg, 45%). TOF MS ES (*m/z*) $[M]^+$ calculated for $C_8H_{13}N_2O_2$, 169.0977, found 169.0978. ^{1}H NMR ($CDCl_3$, 300 MHz): δ ppm 10.34 (s, 1H), 7.57 (m, 1H), 7.30 (s, 1H), 4.69 (t, 2H), 4.05 (s, 3H), 3.69 (s, 3H), 3.10 (t, 2H); ^{13}C NMR ($CDCl_3$, 125 MHz): δ ppm 171.00, 137.74, 123.22, 123.16, 52.35, 45.41, 36.86, 34.65.

3: To a solution of 1,8-diazabicyclo[5.4.0]undec-7-ene (5.48 g, 36 mmol) in acetonitrile (50 mL), methyl 3-bromopropionate (3.9 mL, 36 mmol) was added slowly and the mixture was heated to reflux overnight. The solvent was removed under reduced pressure and the product was purified by column chromatography on silica gel using a gradient starting with 1% methanol in DCM and increasing to 5% methanol in DCM. The desired diazabicycloundecene byproduct was isolated as a colorless liquid (52 mg, < 1%). Note that the yield of nucleophile byproduct **3** was especially low because the addition of DBU and methyl 3-bromopropionate results in the predominant E_2 elimination of bromine to give methyl acrylate. The same E_2 reaction occurs during the synthesis of **1** and **2**, however it is especially pronounced in the presence of DBU. Despite this complication, a sufficient quantity of the model DBU

byproduct **3** was obtained to enable the current study. TOF MS ES (*m/z*) $[M]^+$ calculated for $C_{13}H_{23}N_2O_2$, 239.1760, found 239.1756. ^1H NMR ($CDCl_3$, 300 MHz): δ ppm 3.99 (t, 2H), 3.76 (m, 7H), 3.70 (t, 2H), 3.06 (d, 2H), 2.85 (t, 2H), 2.20 (m, 2H), 1.84 (m, 6H); ^{13}C NMR ($CDCl_3$, 125 MHz): δ ppm 171.08, 167.63, 55.87, 52.25, 49.67, 49.64, 47.36, 33.09, 29.27, 28.52, 25.97, 23.02, 20.15.

General procedure for byproduct reactions with thiolate. Sodium hydride was added to a round-bottom flask under inert atmosphere followed by the addition of anhydrous $CDCl_3$. The solution was cooled down to 0 °C using an ice bath and methyl 3-mercaptopropionate was added to the NaH solution dropwise. The mixture was allowed to stir for 2 h at 0 °C. An equimolar amount of the aza-Michael nucleophile byproduct (**1**–**3**) was added to a separate round-bottom flask under inert atmosphere. A minimal amount of dry $CDCl_3$ was added, and the resulting solution was taken up by syringe and transferred dropwise to the NaH mixture at 0 °C. The combined reaction was stirred and allowed to warm to room temperature overnight. The reaction mixture was passed through a short pad of Celite, concentrated under reduced pressure, and dried further under high vacuum. The residue was diluted with $CDCl_3$ and analyzed by ^1H NMR spectroscopy.

The quantities used for thiolate reactions with nucleophile byproducts **1**–**3** were as follows: DMAP nucleophile byproduct **1** (28.9 mg, 0.1 mmol) was mixed with sodium hydride (60% dispersion in oil) (4.0 mg, 0.1 mmol) and methyl 3-mercaptopropionate (11 μL, 0.1 mmol). MIM nucleophile byproduct **2** (24.9 mg, 0.1 mmol) was mixed with sodium hydride (60% dispersion in oil) (4.0 mg, 0.1 mmol) and methyl 3-mercaptopropionate (11 μL, 0.1 mmol). DBU nucleophile byproduct **3** (42.7 mg, 0.13 mmol) was mixed with sodium hydride (60% dispersion in oil) (5.4 mg, 0.13 mmol) and methyl 3-mercaptopropionate (15 μL, 0.13 mmol). Each reaction resulted in the formation of symmetric thiodipropionate **4**.

Computational Modeling

Computational investigations were performed using the Gaussian16 suite of programs.[14] Structures of stationary points along each reaction mechanism were each subjected to a conformational search by scanning all freely rotating torsional angles at the B3LYP/6-31G(d)[15] level to locate approximate global energy minimum structures. The optimal structure of each stationary point was then optimized to full convergence at the B3LYP/6-31+G(d) level of theory. Approximate transition state geometries were located by scanning along the reaction coordinate(s) corresponding to bond breakage/formation. Each approximate transition state geometry was then subjected to a Berney transition state optimized to full convergence. Transition states were distinguished as having a single imaginary vibrational frequency, whereas all minima had only real vibrational frequencies. Prior computational modeling of thiol-Michael reactions by Houk,[11a] Qi,[11c] and Northrop[11d,12] has shown that geometry optimization at the B3LYP/6-31+G(d) level followed by single-point energy calculations using the M06-2X functional[16] with a large basis set provides reaction energetics that agree well with CBS-QB3 benchmarks. Reaction and transition state enthalpies and free energies reported herein were therefore calculated at the M06-2x/6-311+G(2d,p)//B3LYP/6-31+G(d) level. Reaction energetics were obtained at 298.15 K, 1.0 atm pressure, and in a PCM model[17] of $CHCl_3$ and DMSO solvents.

Acknowledgements

The authors gratefully acknowledge financial support from the National Science Foundation CAREER program (award CHE-1352239) and from Wesleyan University.

Conflict of Interest

The authors declare no conflict of interest.

Keywords: click chemistry · density functional theory · nucleophiles · reaction mechanisms · thiol-Michael reactions

[1] a) D. P. Nair, M. Podgórski, S. Chatani, T. Gong, W. Xi, C. R. Fenoli, C. N. Bowman *Chem. Mater.* **2014**, *26*, 724–744; b) A. B. Lowe *Polym. Chem.* **2014**, *5*, 4820–4870.

[2] a) H. C. Kolb, M. G. Finn, K. B. Sharpless *Angew. Chem. Int. Ed.* **2001**, *40*, 2004–2021; *Angew. Chem.* **2001**, *113*, 2056–2075; b) C. E. Hoyle, C. N. Bowman *Angew. Chem. Int. Ed.* **2010**, *49*, 1540–1573; *Angew. Chem.* **2010**, *122*, 1584–1617; c) P. Espeel, F. E. Du Prez *Macromolecules*, **2015**, *48*, 2–14.

[3] a) M. Podgórski, S. Chatani, C. N. Bowman *Macromol. Rapid Commun.* **2014**, *35*, 1497–1502; b) S. Martens, J. O. Holloway, F. E. Du Prez *Macromol. Rapid Commun.* **2017**, *38*, 1700469.

[4] a) X. Ma, Q. Sun, Z. Zhou, E. Jin, J. Tang, E. Van Kirk, W. J. Murdoch, Y. Shen *Polym. Chem.* **2013**, *4*, 812–819; b) S. Chatani, M. Podgórski, C. Wang, C. N. Bowman *Macromolecules* **2014**, *47*, 4894–4900; c) Z. Zhang, S. Feng, J. Zhang *Macromol. Rapid Commun.* **2016**, *37*, 318–322; d) S. H. Frayne, R. M. Stolz, B. H. Northrop *Org. Biomol. Chem.* **2019**, *17*, 7878–7883.

[5] a) D. P. Nair, N. B. Cramer, J. C. Gaipa, M. K. McBride, E. M. Matherly, R. R. McLeod, R. Shandas, C. N. Bowman *Adv. Funct. Mater.* **2012**, *22*, 1502–1510; b) S. Chatani, C. Wang, M. Podgórski, C. N. Bowman *Macromolecules* **2014**, *47*, 4949–4954; c) W. Xi, A. Aguirre-Soto, C. J. Kloxin, J. W. Stansbury, C. N. Bowman *Macromolecules*, **2014**, *47*, 6159–6165.

[6] a) M. P. Lutolf, J. A. Hubbell *Biomacromolecules* **2003**, *4*, 713–722; b) S. C. Rizzi, J. A. Hubbell *Biomacromolecules* **2005**, *6*, 1226–1238; c) X. Sui, L. van Ingen, M. A. Hempenius, G. J. Vancso *Macromol. Rapid Commun.* **2010**, *31*, 2059–2063; d) S. P. Zustiak, J. B. Leach *Biomacromolecules* **2010**, *11*, 1348–1357; e) K. Peng, I. Tomatsu, B. van den Broek, C. Cui, A. V. Korobko, J. van Noort, A. H. Meijer, H. P. Spaink, A. Kros *Soft Matter* **2011**, *7*, 4881–4887; f) L. Maleki, U. Edlund, A.-C. Albertsson *Biomacromolecules* **2015**, *16*, 667–674; g) N. G. Moon, A. M. Pekkanen, T. E. Long, T. N. Showalter, B. Libby *Polymer* **2017**, *125*, 66–75.

[7] a) C. Wang, S. Chatani, M. Podgórski, C. N. Bowman *Polym. Chem.* **2015**, *6*, 3758–3763; b) D. Konetski, A. Baranek, S. Mavila, X. Zhang, C. N. Bowman *Soft Matter* **2018**, *14*, 7645–7652.

[8] a) T. H. Ho, M. Levere, J.-C. Soutif, V. Montembault, S. Pascual, L. Fontaine *Polym. Chem.* **2011**, *2*, 1258–1260; b) W. Tang, M. L. Becker, *Chem. Soc. Rev.* **2014**, *43*, 7013–7039; c) B. Bernardim, P. M. S. D. Cal, M. J. Matos, B. L. Oliveira, N. Martínez-Sáez, I. S. Albuquerque, E. Perkins, F. Corzana, A. C. B. Burtoloso, G. Jiménez-Osés, G. J. L. Bernardes *Nat. Commun.* **2016**, *7*, 13128; d) Y. Sun, H. Liu, L. Cheng, S. Zhu, C. Cai, T. Yang, L. Yang, P. Ding *Polym. Int.* **2018**, *67*, 25–31.

[9] a) H. Seto, M. Takara, C. Yamashita, T. Murakami, T. Hasegawa, Y. Hoshino, Y. Miura *ACS Appl. Mater. Interfaces* **2012**, *4*, 5125–5133; b) R. Tedja, A. H. Soeriyadi, M. R. Whittaker, M. Lin, C. Marquis, C. Boyer, T. P. Davis, R. Amal *Polym. Chem.* **2012**, *3*, 2743–2751.

[10] a) J. W. Chan, C. E. Hoyle, A. B. Lowe, M. Bowman *Macromolecules* **2010**, *43*, 6381–6388; b) G.-Z. Li, R. K. Randev, A. H. Soeriyadi, G. Rees, C. Boyer, Z. Tong, T. P. Davis, C. R. Becer, D. M. Haddleton *Polym. Chem.* **2010**, *1*, 1196–1204; c) W. Xi, C. Wang, C. J. Kloxin, C. N. Bowman *ACS Macro Lett.* **2012**, *1*, 811–814; d) L.-T. Nguyen, M. T. Gokmen, F. E. Du Prez *Polym. Chem.* **2013**, *4*, 5527–5536; e) S. Chatani, D. P. Nair, C. N. Bowman *Polym. Chem.* **2013**, *4*, 1048–1055; f) S. H. Frayne, R. R. Murthy, B. H. Northrop *J. Org. Chem.* **2017**, *82*, 7946–7956; g) S. Huang, J. Sinha, M. Podgórski, X. Zhang, M. Claudino, C. N. Bowman *Macromolecules* **2018**, *51*, 5979–5988.

[11] a) E. H. Krenske, R. C. Petter, Z. Zhu, K. N. Houk *J. Org. Chem.* **2011**, *76*, 5074–5081; b) R. M. Stolz, B. H. Northrop *J. Org. Chem.* **2013**, *78*, 8105–8116; c) C. Wang, C. Qi *Tetrahedron* **2013**, *69*, 5348–5354; d) B. H. Northrop, S. H. Frayne, U. Choudhary *Polym. Chem.* **2015**, *6*, 3415–3430; e) G. B. Desmet, M. K. Sabbe, D. R. D'hooge, P. Espeel, S. Celasun, G. B. Marin, F. E. Du Prez, M. F. Reyniers *Polym. Chem.* **2017**, *8*, 1341–1352.
[12] S. H. Frayne, B. H. Northrop *J. Org. Chem.* **2018**, *83*, 10370–10382.
[13] The direct S_N2 displacement by thiolate (Scheme 2) is a single step process while deprotonation by thiolate followed by elimination (Scheme 2; is a two-step mechanism where the first step (deprotonation) is rate-determining. Transition state theory therefore predicts that the difference in likelihood of following these two pathways will be proportional to the difference in relative Gibbs free energy of the two competitive transition states.
[14] Gaussian 16, Revision C.01, M. J. Frisch, G. W. Trucks, H. B. Schlegel, G. E. Scuseria, M. A. Robb, J. R. Cheeseman, G. Scalmani, V. Barone, G. A. Petersson, H. Nakatsuji, X. Li, M. Caricato, A. V. Marenich, J. Bloino, B. G. Janesko, R. Gomperts, B. Mennucci, H. P. Hratchian, J. V. Ortiz, A. F. Izmaylov, J. L. Sonnenberg, D. Williams-Young, F. Ding, F. Lipparini, F. Egidi, J. Goings, B. Peng, A. Petrone, T. Henderson, D. Ranasinghe, V. G. Zakrzewski, J. Gao, N. Rega, G. Zheng, W. Liang, M. Hada, M. Ehara, K. Toyota, R. Fukuda, J. Hasegawa, M. Ishida, T. Nakajima, Y. Honda, O. Kitao, H. Nakai, T. Vreven, K. Throssell, J. A. Montgomery, Jr., J. E. Peralta, F. Ogliaro, M. J. Bearpark, J. J. Heyd, E. N. Brothers, K. N. Kudin, V. N. Staroverov, T. A. Keith, R. Kobayashi, J. Normand, K. Raghavachari, A. P. Rendell, J. C. Burant, S. S. Iyengar, J. Tomasi, M. Cossi, J. M. Millam, M. Klene, C. Adamo, R. Cammi, J. W. Ochterski, R. L. Martin, K. Morokuma, O. Farkas, J. B. Foresman, D. J. Fox, *Gaussian*, Inc., Wallingford CT, 2016.
[15] a) C. Lee, W. Yang, R. G. Parr *Phys. Rev. B.* **1988**, *37*, 785–789; b) A. D. Becke *J. Chem. Phys.*, **1993**, *98*, 1372–1377; c) A. D. Becke *J. Chem. Phys.* **1993**, *98*, 5648–5652.
[16] Y. Zhao, D. G. Truhlar *Theor. Chem. Acc.* **2008**, *120*, 215–241.
[17] a) S. Miertus, E. Scrocco, J. Tomasi *Chem. Phys.* **1981**, *55*, 117–129; b) M. Cossi, V. Barone, R. Cammi, J. Tomasi *Chem. Phys. Lett.* **1996**, *255*, 327–335.

Manuscript received: August 20, 2020
Revised manuscript received: October 28, 2020